Chapter 2

Review of pervious experimental work

2-1 $ACu_3Ti_4O_{12}$

It was well known that the oxides with the perovskite structure have the ability to produce high dielectric constants leading to many important applications. The perovskite-like $ACu_3Ti_4O_{12}$ family of materials were first found in 1967,[28] and their accurate structures were determined from neutron powder diffraction data in 1979.[29] $CaCu_3Ti_4O_{12}$ (CCTO) reveals a perovskite-related structure (pace group *Im3*, No. 204) which are extensions of the classic perovskite compound-ABO_3 shown in Fig. 2 – 1. It is an unusual variation the cubic perovskite structure with the tilting TiO_6 to produce a square planar coordination of Cu^{2+}. Temperature-dependent structural parameters and dielectric properties of these compounds were examined by M. A. Subramanian *et al*. in 2000.[7] The X-ray powder diffraction data at 35 K and 100 K show no evidence for any structural phase transition of CCTO, which remains cubic and centric structure down to 35 K.

Temperature-dependent dielectric properties of these compounds were also examined by M. A. Subramanian *et al*. in 2000.[7] The ε_1(100 kHz) value of CCTO is ～10286 from 300 K to 573 K and the other substitutions of Ca such as Cd, La, and Bi all lower the ε_1(100 kHz) value at room-temperature. To illustrate the giant dielectric constants, they compare these with $BaTiO_3$ ones. With decreasing temperature, the Ti^{4+} ions displace toward one, two, and finally three oxygen anions to produce respectively the tetragonal, orthorhombic, and rhombohedral ferroelectric

structures, leading a suggestion that the high permittivity of CCTO may arise from local dipole moments associated with off-center displacement of Ti ions but the pure ferroelectric transition is frustrated by the TiO_6 octahedral tilt.

C. C. Homes *et al*. in 2001 presented the temperature dependent ε_1 and dissipation factor (or loss component) at different frequencies.[14] In Fig. 2 – 2, they showed that the ε_1(~kHz) values $\sim 8\times 10^4$ near a constant between 100 K and 600 K, and rapidly decrease (~100) below 100 K. However, the low-frequency ε_1 values at 300 K (~70) estimated from optical data is not consistent with their microwave ones (~10^5). They suggest that the Lorentz model results in a seriously overdamped oscillator ($\gamma \gg \omega_0$). It indicates that this physical process is dominated by relaxation effect that naturally favors a Debye model for the relaxation time of a dipole ($P(t) = P_0 e^{-t/\tau}$), where P_0 is the dipole moment and τ is the characteristic relaxation time. The frequency response for the dielectric function is written as

$$\varepsilon(\omega) = \varepsilon_\infty + \frac{P_0\tau(1+i\omega\tau)}{1+(\omega\tau)^2}, \qquad (2\text{-}1\text{-}1)$$

and $P_0 = \varepsilon_0 - \varepsilon_\infty$. The fitting results are shown in Fig 2 – 3 (a) as a solid line. Figure 2 – 3 (b) shows the log of the relaxation time τ versus $1/T$, where $\tau = \tau_0 e^{U/k_B T}$, the parameter U = 54 m eV (~630K), and τ_0 = 84 ns.

Impedance spectroscopy data of CCTO ceramics were published by D.C. Sinclair *et al*.[30] The impedance spectroscopy data can often be modeled by an ideal equivalent circuit including two parallel RC elements connected in series, as shown in Fig. 2 – 4. The two parallel RC elements connected in series consist of one RC element for the bulk and the other for the grain boundary response.[31] The formation

of grain boundary is possibly due to annealing after high strain. The grain and grain boundary responses model alternatively well simulate the behavior that ε_1(～kHz) drop to ～100 below 100 K. It provides evidence that the microstructure of CCTO is electrically heterogeneous and makes up of semiconducting grains with insulating grain boundaries. The giant dielectric phenomenon results form an internal barrier layer capacitance (IBLC) instead of an intrinsic property associated with the crystal structure. From now on, the Maxwell-Wagner relaxation model, which describes the interfacial polarization due to capacitive barrier layers associated with grains and grain boundaries, is always used to illustrate the nature of giant ε_1 values and the interesting temperature-dependent behavior of CCTO.

Far-infrared spectra of a single-crystalline CCTO were first presented by C. C. Homes *et al*. [14] The low-temperature optical conductivity data below 300 cm^{-1} reveal interesting red shifts and remarkable increases in intensity and linewidth possibly due to the charges redistribution. As shown in Fig. 2 – 5,[10] the far-infrared conducttivity of $CdCu_3Ti_4O_{12}$ (CdCTO) ceramics show similar red shifts and increases in intensity as CCTO. However, the effective charges of CdCTO is lower than those of CCTO at varied temperature due to the higher Pauling electronegativity of Cd atom (～1.7) in comparison of that of Ca (～1).[10]

The magnetic properties of CCTO were also investigated.[32,33] An antiferromagnetic phase transition was found near 25 K in CCTO. More detailed information about magnetic susceptibility measurements will be discussed in Chapter 4. The magnetic structure was also determined by neutron scattering measurements taken by Y.J. Kim *et al*.[33] Figure 2 – 6 presents the arrangement of Cu^{2+} spins parallel to the [111] direction. J_1, J_2, and J_3 are the effective exchange integrals between nearest,

next-nearest, and third-nearest neighbors. It should be noted that J_1 and J_3 are the antiferromagnetically correlated, whereas the J_2 interaction is ferromagnetic.

The first-principle calculation of CCTO was performed by using density-functional theory (DFT) within the local spin-density approximation (LSDA).[11] The calculated phonon frequencies were in good agreement with the experimental measurements with the static dielectric constant ～40.

2-2 $CaMnO_3$

$CaMnO_3$ is of the parent compound of the manganese oxides $La_xCa_{1-x}MnO_3$, which were first investigated by G.H. Jonker and J.H. Van Santen.[34] Figure 2 – 7 illustrates the crystallographic and magnetic phase transitions of $La_xCa_{1-x}MnO_3$ ($0.0 \leq x \leq 0.2$).[35] The phase diagram shows orthorhombic antiferromagnetic (AFM) for x up to 0.16, but that less than 20% of the x = 0.16 sample is actually in this state at low temperature. With the composition x ～0.1, the manganites $La_xCa_{1-x}MnO_3$ were found the CMR properties.[2] Neutron diffraction studies of $La_xCa_{1-x}MnO_3$ (x = 0 to 1) at different temperature were made by E. O. Wollan and W. C. Koehler.[34] They also found a antiferromagnetic phase transition in $CaMnO_3$ with Néel temperature (T_N) ～110 K. Below 110 K, the ordering of Mn ions of $CaMnO_3$ is identified as G-type antiferromagnetic structure. Figure 2 – 8 presents the ideal G-type antiferromagneitc arrangement. Each Mn^{4+} ion is surrounded by six Mn^{4+} neighbors whose spins are antiparallel to the given ion. The structure can be thought of as consisting of two interpenetrating face centered lattices with opposite spin orientation.

The crystal structure of pure $CaMnO_3$ at room-temperature was once determined

by J. BLASCO *et al*.[36] In their assignments, they had studied crystal structures of $Tb_{1-x}Ca_xMnO_3$ by using x-ray and neutron diffraction. It turns out that $CaMnO_3$ is a single-phase compound indexed in the orthorhombic *Pbnm* space group (standard setting *Pnma*, No. 62). Figure 2 – 9 shows the crystal structure of $CaMnO_3$, which is one of the most common distorted structures derived from the cubic perovskite.

The temperature-dependent X-ray powder diffraction and Raman scattering measurements of La-doped $CaMnO_3$ were done by E. Granado *et al*.[37] The orthorhombic lattice parameters (space group *Pbnm*), and the unit cell volume of $CaMnO_3$ at varied temperature are shown in Fig. 2 – 10. It is noted that no structural anomalies near the Néel temperature are observed except slight changes of the lattice constants. Interestingly, in undoped $CaMnO_3$ the softening of the bending vibrations of octahedra at 470 and 490 cm^{-1} and hardening of the stretching mode at 585 cm^{-1} are found along with small softening of the external mode near 260 cm^{-1}. These phonon anomalies are attributed to the strong spin-phonon coupling.

Optical studies of polycrystalline[17,18,38] $CaMnO_3$ and single-crystal[16,39] $CaMnO_{3-\delta}$ samples were investigated. The optical conductivity of single-crystal $CaMnO_{3-\delta}$ revealed two electronic transition absorption at 2.2 eV and 3.1 eV, which are associated with superposition of the charge-transfer transitions $O(2p)\rightarrow Mn(e_g)\uparrow$ and $O(2p)\rightarrow Mn(t_{2g})\downarrow$. Intensity of the peak at 2.2 eV depends on Mn contents. The peak at 2.2 eV was not observed in the optical conductivity spectra of $CaMnO_3$ polycrystalline samples. The goal of the optical studies is to determine peculiarities of the fundamental absorption spectra and interaction of light with the charge carriers in $CaMnO_3$.

2-3 Sr_2YRuO_6

The room temperature crystal structure and magnetic properties of distorted perovskite Sr_2YRuO_6 had been undertaken by P. D. Batle *et al*.[40] Figure 2 – 11 shows the crystal structure of Sr_2YRuO_6 at room temperature refined by using neutron powder diffraction data. It exhibits the monoclinic space group $P2_1/n$ crystal structure with unit cell parameters a = 5.76 Å, b = 5.77 Å, c = 8.15 Å, and β = 90.23°. R–O and Y–O octahedral are all titled away from their ideal cubic orientation with long Y–O (2.2 Å) and a short Ru–O (1.95 Å). Each Ru–O octahedra shares a single O atom with each neighboring Y–O octahedra. Sr_2YRuO_6 is an antiferromagnetic insulator with T_N ~26 K. Figure 2 – 12 shows the spin arrangement of magnetic structure of Sr_2YRuO_6 with the pseudocubic $\sqrt{2}a \times \sqrt{2}b \times$ c unit cell. It includes ferromagnetic (001) plane and antiferromagnetically coupled along [001]. The crystal structure along with magnetization direction from muon spin rotation (μSR) data is also shown in Fig. 2 – 13.[4] There are two important antiferromagnetic exchange interactions: (a) the π superexchange between the nearest Ru ions is carried out via a Ru-O-O-Ru linkage, and (b) the σ superexchange via a Ru-O-Y-O-Ru linkage. However, the Y ions are not expected to play a significant role in the magnetic superexchange because they are fully ionized and provide no accessible orbitals necessary to participate in superexchange. Sr_2RuYO_6 can be thus considered as consisting of tilted RuO6 octahedra which are connected via two bridging O atoms.

The magnetic susceptibility and magnetization measurements of single crystals Sr_2RuYO_6 were performed by G. Cao *et al*.[21] Figure 2 – 14 shows ZFC and FC magnetic susceptibility at varied temperature for different magnetic fields (H = 0.02, 0.5, and 4 T) below 60 K. At H = 0.02 T, the magnetic susceptibility reveals a sharp

shape similar to that of a spin glass. With increasing applied magnetic field, the magnetic transition is getting broad due to the weak ferromagnetism. The magnetic susceptibility of Sr_2RuYO_6 with applied H parallel to *a* and *c* axes are similar due to no significant anisotropy in Sr_2RuYO_6 below Néel temperature.

First-principles calculations of Ru-based perovskites were calculated in 1997 by I. I. Mazin.[41] Density of states along with tight-binding analysis of antiferromagnetic $Sr_2YRuCuO_6$ is presented in Fig. 2 – 15. The O states between –1 and 1 eV relative to the Fermi energy (E_F) hybridize with the Ru 4*d* (t_{2g}), and the states between 2.5 and 4 eV are related to the Ru 4*d* (e_g).

Optical reflectance and Raman scattering studies of a series of $Sr_2Y(Ru_{1-u}Cu_u)O_6$ polycrystalline samples were done previously in our group.[5] The optical conductivity of polycrystalline Sr_2YRuO_6 exhibited four electronic absorptions related to the transitions between the Ru 4*d* states and O(2*p*)→Ru(3*d*). The temperature-dependent Raman-scattering data of Sr_2YRuO_6 revealed the red shifts of the apical oxygen phonon mode below Néel temperature possibly due to the strong spin-phonon coupling effects.

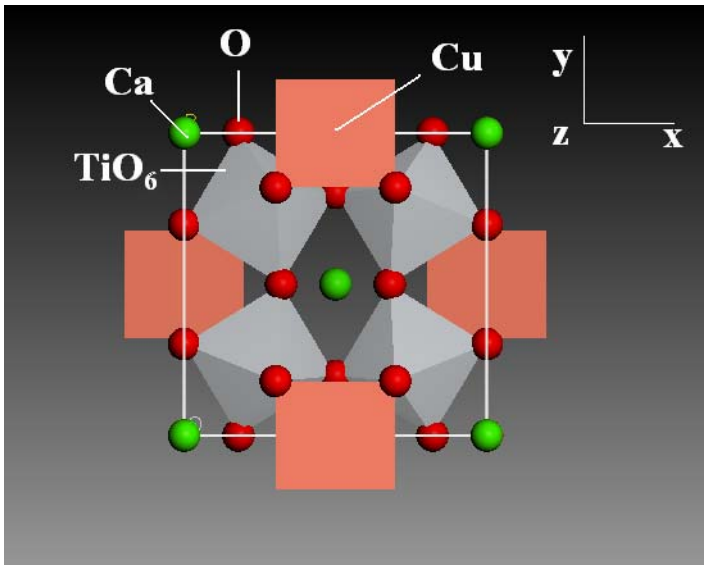

Fig. 2 – 1. The structure of CCTO with TiO_6 octahedra, Cu atoms bonded with four oxygen atoms, and Ca atoms without bonds.[8]

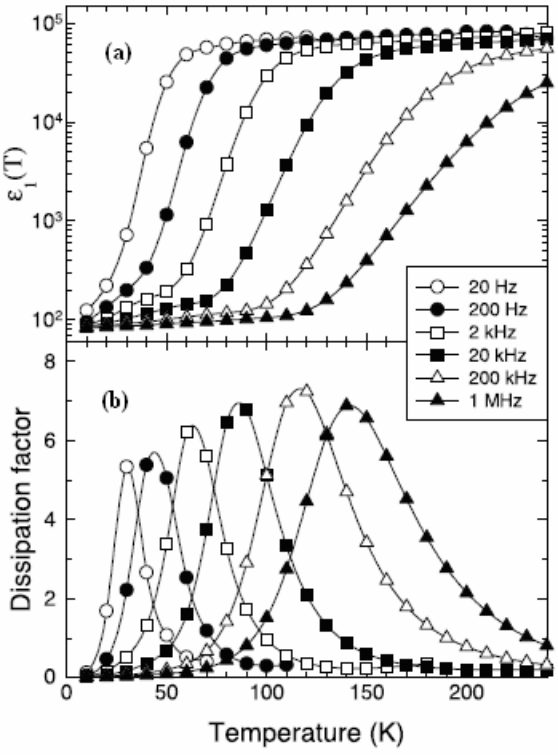

Fig. 2 – 2. The temperature dependent (a) ε_1 and (b) dissipation factor (or loss component) of a single-crystalline CCTO at different frequencies.[14]

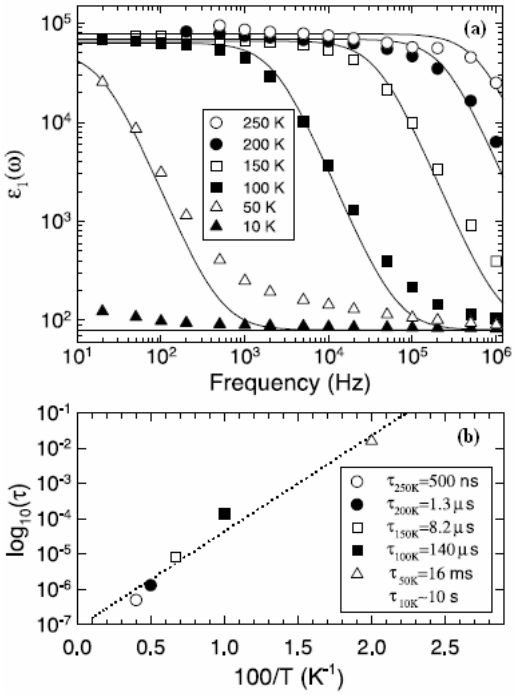

Fig. 2 – 3. (a) The frequency dependence of the ε_1 values of CCTO between 20 Hz and 1 MHz at several temperature. The solid lines are estimated by the Debye model. (b) The log of the relaxation time τ versus $1/T$ along with the dot lines evaluated form the equation ($\tau = \tau_0 e^{U/k_B T}$).[14]

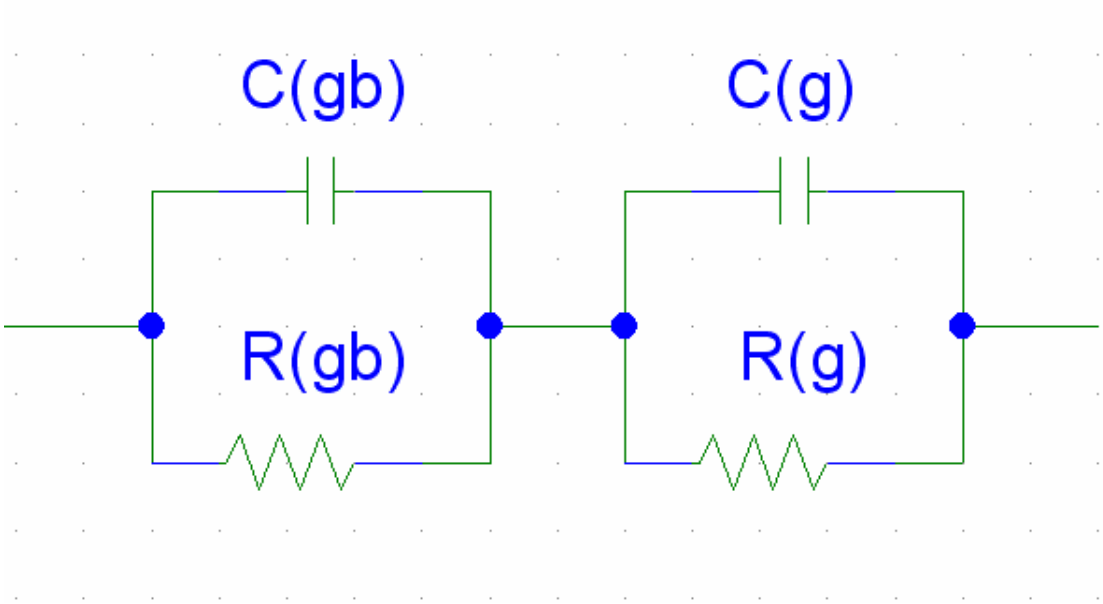

Fig. 2 – 4. The equivalent circuit with two parallel RC elements in series.[6,42]

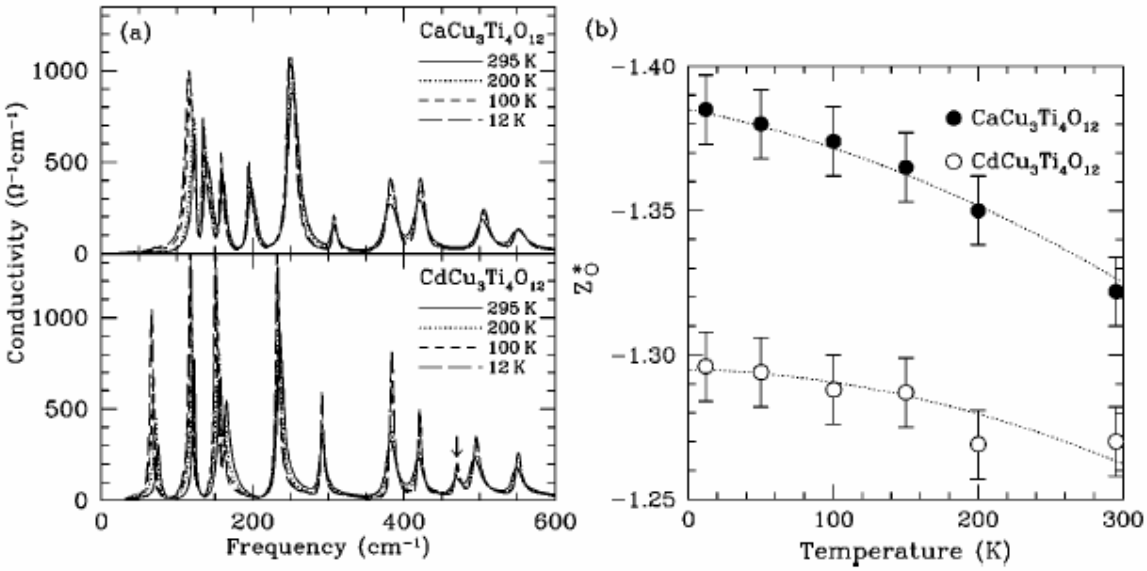

Fig. 2 – 5. The temperature-dependent far-infrared conductivity spectra and the effective charge per oxygen atom (Z_O^*) of CCTO and CdCTO.[10]

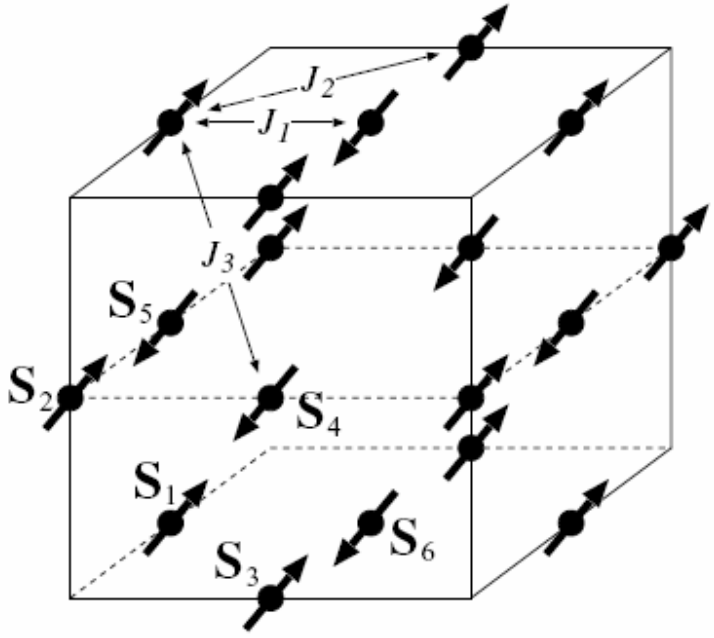

Fig. 2 – 6. The magnetic structure of Cu^{2+} spins in CCTO. Spins are parallel to the [111] crystallographic direction.[33]

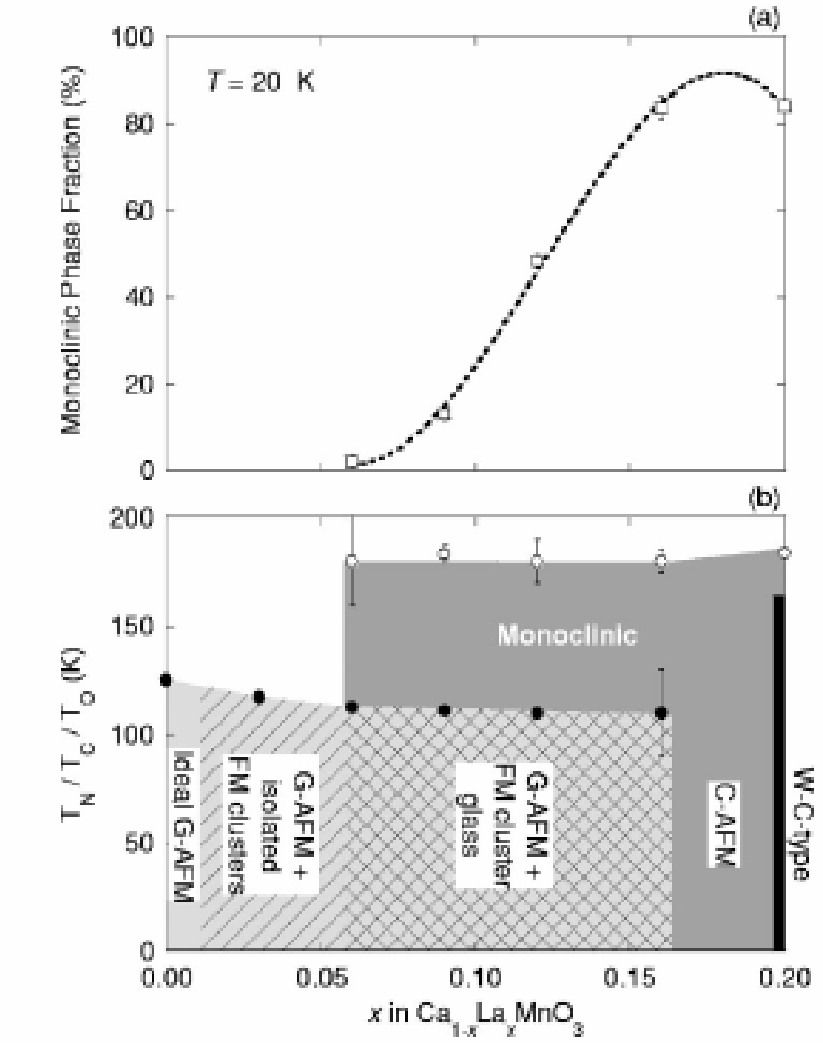

Fig. 2 – 7. (a) Refined monoclinic phase fraction at 20 K as a function of x; (b) crystallographic and magnetic phase transitions of $Ca_{1-x}La_xMnO_3$ ($0.0 \leq x \leq 0.2$) determined from NPD data.[35]

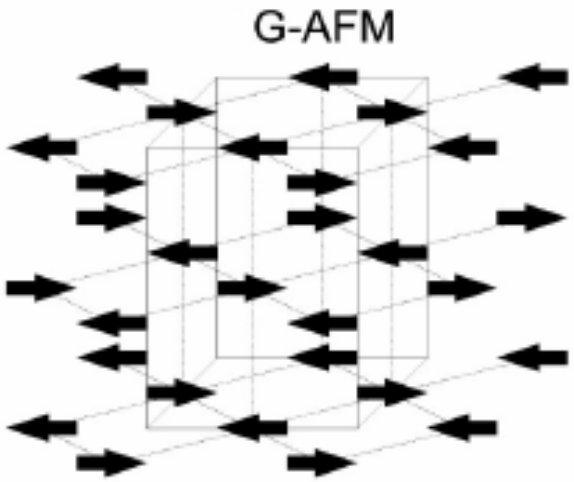

Fig. 2 – 8. The magnetic structure of Mn^{4+} ions in G-type antiferromagnetic $CaMnO_3$.[35]

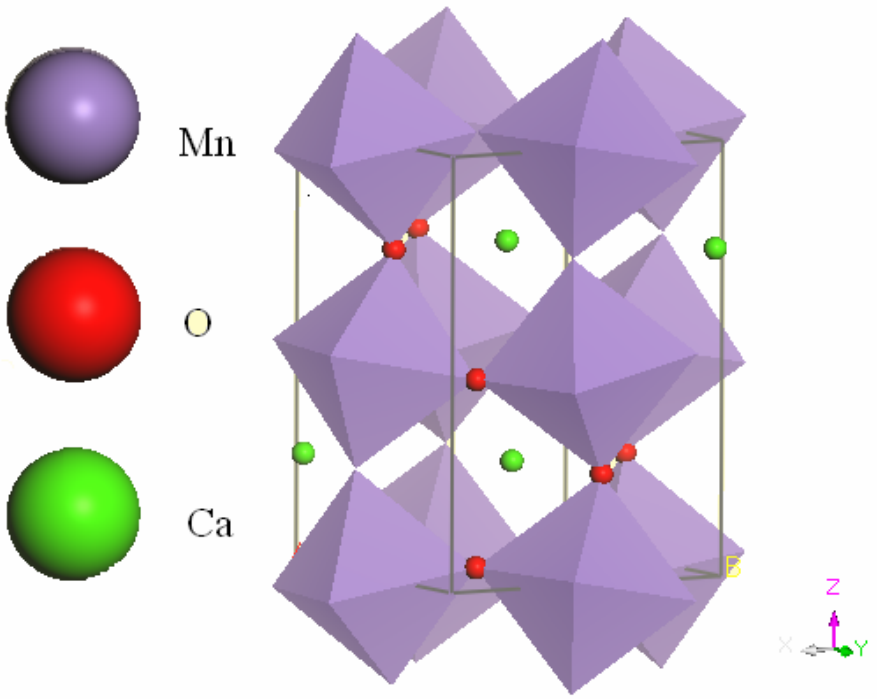

Fig. 2 – 9. The *Pbnm* crystal structure of $CaMnO_3$ at room temperature with purple MnO_6 octahedra and green Ca atoms.[36]

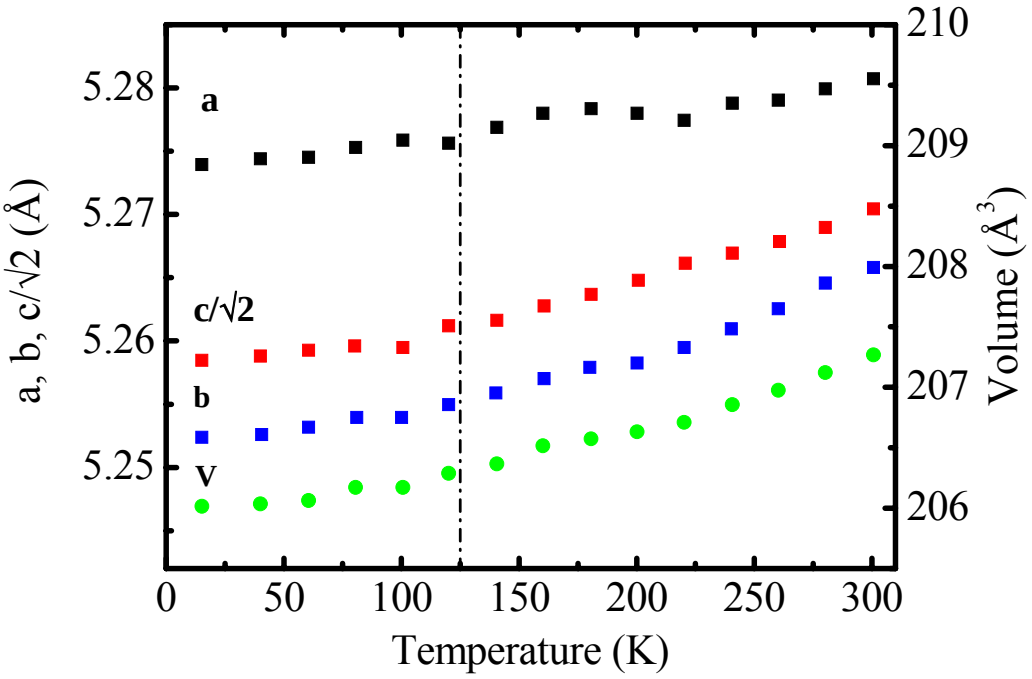

Fig. 2 – 10. The lattice parameters and unit cell volume at varied temperature for $CaMnO_3$.[37]

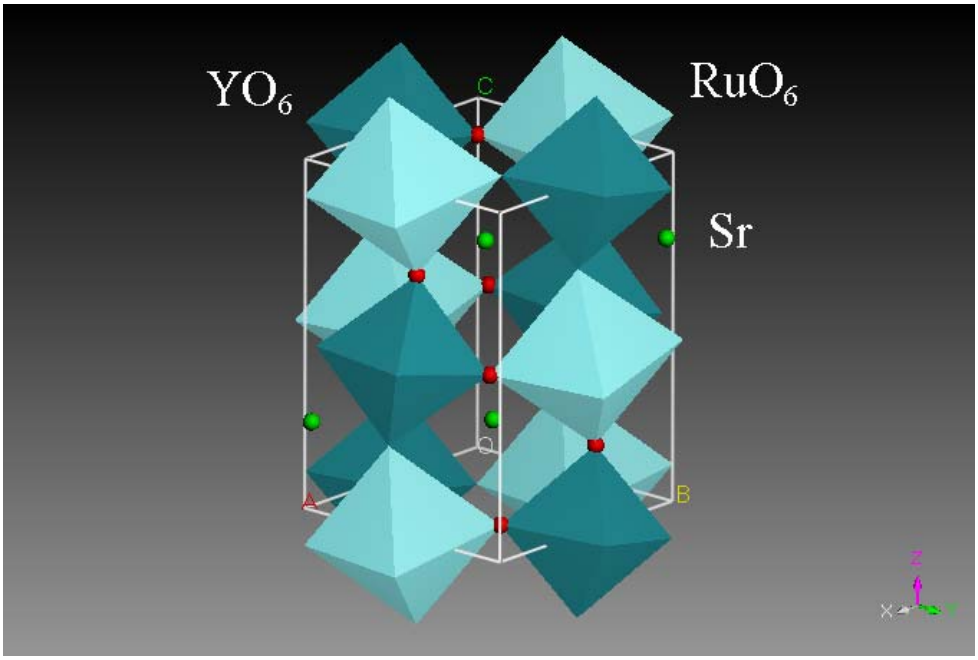

Fig. 2 – 11. The *P2₁/n* crystal structure of Sr_2YRuO_6 at room temperature with RuO_6 and YO_6 octahedra and green Sr atoms.[40]

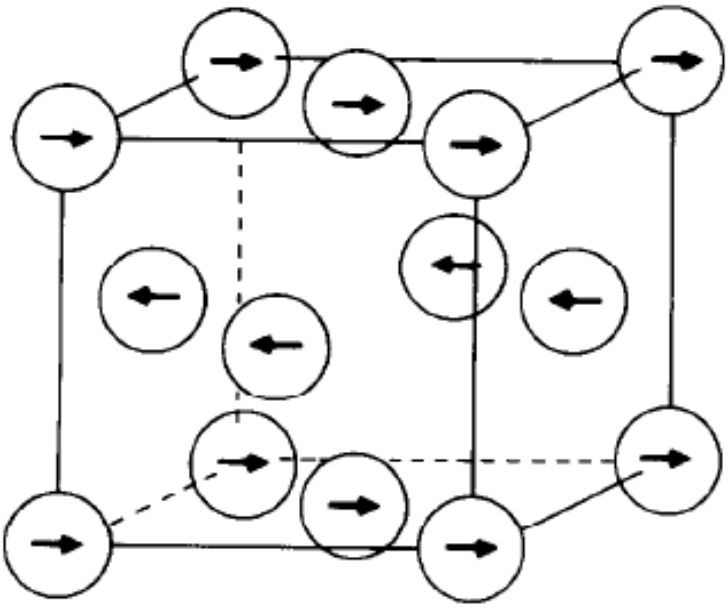

Fig. 2 – 12. The magnetic unit cell of Sr_2YRuO_6. Only ruthenium ions are shown.[40]

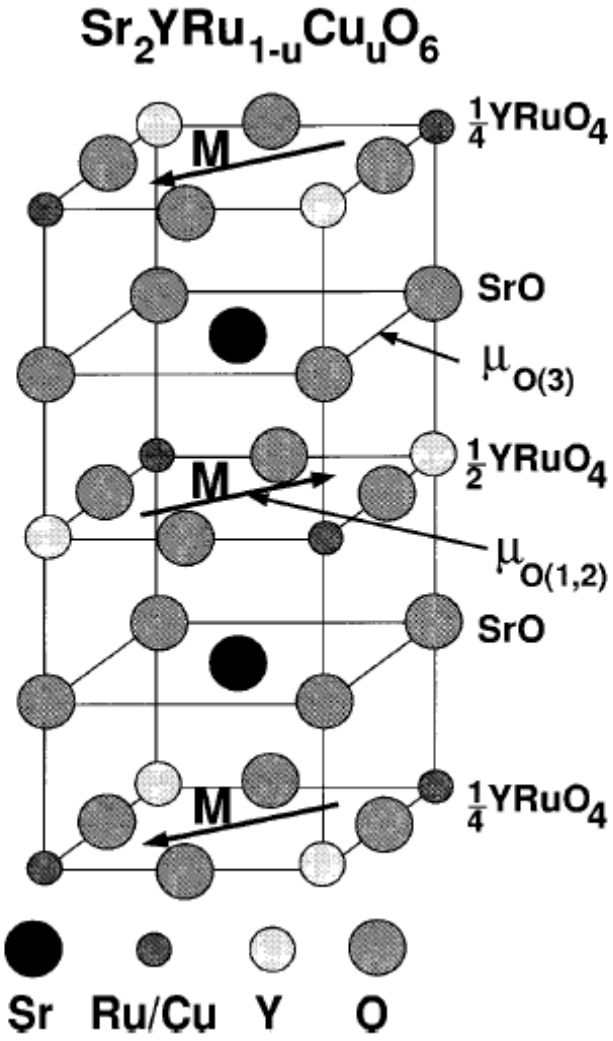

Fig. 2 – 13. The crystal structure of $Sr_2Y(Ru_{1-u}Cu_u)O_6$. The arrows along the [110] direction indicate the magnetization direction in the layered antiferromagnetic structure.[4]

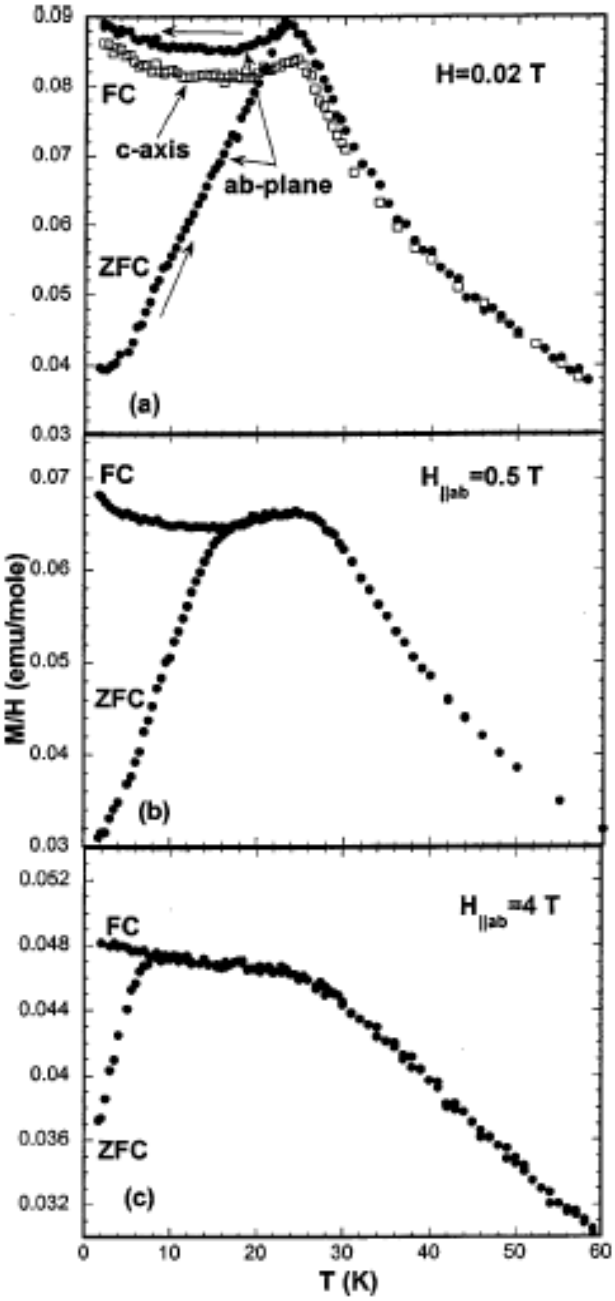

Fig. 2 – 14. Zero-field-cooled (ZFC) and field-cooled (FC) magnetic susceptibility of single-crystal Sr_2YRuO_6 at temperature region form 4 to 60 K along with applied field (a) $H_{\parallel ab}$ = 0.02 T, (b) 0.5 T, and (c) 4 T. Field-cooled magnetic susceptibility for the c axis is also plotted in (a).[21]

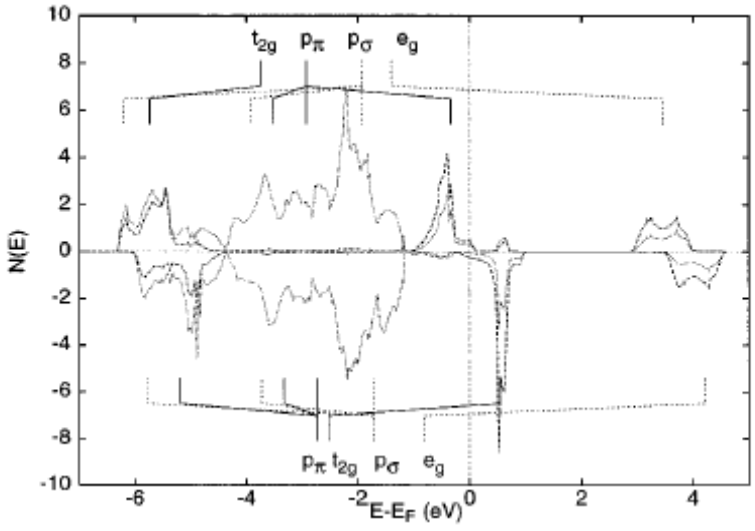

Fig. 2 – 15. Partial density of states along with tight-binding analysis of antiferromagnetic Sr_2YRuO_6. The dotted line is Fermi energy.[41]